Processing and Application of Ceramics 15 [3] (2021) 306–313
https://doi.org/10.2298/PAC2103306S

Thermophysical performances of $(Sm_{1-x}Lu_x)_3TaO_7$ (x = 0, 0.1, 0.3 and 0.5) ceramics

Weiwei Sang[1,2], Hongsong Zhang[2,*], Huahui Chen[1,*], Bin Wen[2], Xinchun Li[2], Mengwei Li[2]

[1]*School of Mechanical Electronic & Information Engineering, China University of Mining & Technology-Beijing, Beijing 10083, PR China*
[2]*School of Mechanical Engineering, Henan University of Engineering, 451191, PR China*

Received 27 April 2021; Received in revised form 12 July 2021; Accepted 4 September 2021

Abstract

To optimize thermophysical performances, Sm_3TaO_7 was doped with Lu^{3+} and pressureless sintered at 1600 °C. It was shown that Sm^{3+} is partly substituted by Lu^{3+} cations and the $(Sm_{1-x}Lu_x)_3TaO_7$ ceramics with a single pyrochlore structure are obtained. With increasing x value from 0 to 0.5, the band gap increases gradually from 4.677 to 4.880 eV. Owing to the enhanced phonon scattering caused by Lu^{3+} doping, the thermal conductivities at 800 °C of the prepared samples are in the range of 0.95–1.44 $W{\cdot}K^{-1}{\cdot}m^{-1}$. It was also confirmed that the phase transition is restrained effectively by substituting Sm^{3+} with Lu^{3+}. Due to the reduction of crystal lattice energy and average electro-negativity difference, the thermal expansion coefficient (TEC) is heightened with increasing Lu content. TEC achieves the highest value (10.45×10^{-6} K^{-1} at 1200 °C) at the equal molar ratio between Sm^{3+} and Lu^{3+} cations (i.e. x = 0.5), which is much higher than those of 7YSZ and $Sm_2Zr_2O_7$ ceramics.

Keywords: *$(Sm,Lu)_3TaO_7$ ceramics, thermal barrier coatings, thermal properties*

I. Introduction

Increased working efficiency of gas turbines and spacecraft engines can be achieved by thermal-barrier coatings (TBCs) having more effective thermal insulation for key metallic components at high-temperatures. Due to the inherent phase-transformations and enhanced shrinkage during sintering of 7–8 wt.% Y_2O_3-stabilized ZrO_2 (7YSZ) above 1200 °C, the current YSZ thermal barrier coatings cannot undertake long-term applicability [1–7]. Therefore, it is necessary to explore novel candidates for TBCs with excellent thermophysical properties.

Recently, rare earth tantalate compounds with formula RE_3TaO_7 have drawn extensive attention due to their excellent thermophysical properties [8–12]. For example, it is reported that thermophysical properties of Eu_3TaO_7 can be improved by ZrO_2 addition, which weakens the bonding strength of Eu_3TaO_7 [8]. Gd_3TaO_7 has lower thermal conductivity than YSZ, which can be reduced further by La^{3+} substitution for Gd^{3+} [9]. Thermal conductivity of Gd_3TaO_7 is also decreased by Al_2O_3 addition, while coefficients of thermal expansion for $(Al_xGd_{1-x})_3TaO_7$ are in the same order with that of 7–8 wt.% YSZ [10]. Compared to La_3TaO_7, La_2AlTaO_7 has relatively low thermal expansion coefficient and high thermal conductivity [11].

In addition, it is found that TiO_2 addition can slightly reduce thermal conductivity of Sm_3TaO_7, while the phase transition cannot be suppressed effectively, and the reason for this phase transition in Sm_3TaO_7 is not explained [12]. It has been reported that phase transition can be restrained via cation substitution with the same chemical valence [13,14]. For example, the phase transition can be successfully moved to below room temperature with increasing Fe^{3+} substitution with Sc^{3+} in $Fe_{2-x}Sc_xMo_3O_{12}$, which induces no phase transition at operating temperature [13]. The phase transition from orthorhombic phase to tetragonal phase is suppressed by Cr^{3+} substitution for Mn^{3+} in $LiMn_2O_4$ [14]. The influence of RE^{3+} substitution for Sm on crystal-lattice and thermophysical properties of Sm_3TaO_7 ceramics has not been studied openly up to now. Therefore, the $(Sm_{1-x}Lu_x)_3TaO_7$ (*x* = 0, 0.1, 0.3 and 0.5) ceramics were

* Corresponding author: tel: +8615188384571,
e-mail: *zhsandchen@126.com* (H. Zhang)
chh@cumtb.edu.cn (H. Chen)

processed and their microstructure and thermophysical properties were examined in the present paper.

II. Experimental

In this study, the $(Sm_{1-x}Lu_x)_3TaO_7$7 ceramics (where $x = 0, 0.1, 0.3$ and 0.5) were prepared through solid state sintering technique using Sm_2O_3, Lu_2O_3 and Ta_2O_5 as raw oxides. All raw oxides were bought from Hzrare Chem. Co. Ltd, Guangdong, China, whose purities are greater than 99.9%. The selected precursors were calcined at 1000 °C in air for 120 min to completely remove of adsorbed H_2O and CO_2. Subsequently, the raw reactants were weighted in stoichiometric ratio and ground fully for 1 h in an agate mortar. After 200-mesh standard sieving, the mixtures were pressed at 12 MPa for 5 min by hydraulic pressing, and then at 200 MPa for 10 min by cold isostatic pressing to form green samples. Finally, the bulk samples were obtained by pressureless sintering at 1600 °C for 12 h in air.

Crystal structure of the bulk specimens was confirmed employing X-ray diffractometer (XRD, D/Max-2500M, Rigaku, Japan). Raman spectra of the bulk specimens were collected by a laser Raman spectroscopy (inVia Reflex, Renishaw, England). Subsequently, surface microstructure of the sintered samples was observed by scanning electron microscope (SEM, Sigma 500, Zeiss, Germany). Elemental composition was analysed via an energy dispersive spectroscopy (EDS, Oxford, England). The bulk density (ρ) was confirmed by the Archimedes method and porosity (ϕ) was obtained by the formula $\phi = 1 - \rho/\rho_0$ (ρ_0 is the theoretical density).

Reflectance (R_∞) of the samples between 200 and 800 nm wavelength using $BaSO_4$ as reference was obtained by UV-Vis scanning spectrophotometer (UV-3600plus, Shimadzu, Japan). Then the absorption (A) and Kubelka-Munk remission function $F(R_\infty)$ were converted from reflectance by the following equations, respectively:

$$A = -\log R_\infty \tag{1}$$

$$F(R_\infty) = \frac{(1 - R_\infty)}{2R_\infty} \tag{2}$$

The band gap (E_g) of the samples could be derived from the Kubelka-Munk method [15]. Thermal diffusivity (λ) of the $(Sm_{1-x}Lu_x)_3TaO_7$ samples was tested by a laser flash diffusivity thermal instrument (LFA 1000, German Linseis); the specimen dimension was about 1 mm in thickness and 12.7 mm in diameter. To prevent the laser penetrating through the translucent specimens at high temperatures, both the back and front faces of the samples were coated with a thin graphite film. Based on the reference specific heat values of Sm_2O_3, Lu_2O_3 and Ta_2O_5, the specific heat capacity (C_p) of specimens was computed by the Neumann-Kopp rule [16]. The thermal conductivity (k) of bulk samples was calculated according to thermal diffusivity (λ), density (ρ) and specific heat capacity (C_p) by Eq. 3. In order to eliminate influence of pore content (ϕ), the actual thermal conductivity (k_0) was computed by Eq. 4 [17,18].

$$k = C_p \cdot \lambda \cdot \rho \tag{3}$$

$$\frac{k}{k_0} = 1 - \frac{4}{3}\phi \tag{4}$$

Thermal expansion performance of specimens (25 mm × 4 mm × 3 mm) was investigated by the thermal expansion apparatus (DIL 402 C, Netzsch, Germany) between 50 and 1200 °C.

III. Results and discussion

3.1. Crystal structure and microstructure

XRD patterns of the $(Sm_{1-x}Lu_x)_3TaO_7$ ceramics (Fig. 1a) are consistent with PDF #38-1412 and eleven diffraction peaks can be indexed to (111), (311), (222), (400), (511), (440), (622), (444), (800), (662) and (840) planes. The intense and sharp peaks of the patterns indicate the high crystallinity of the synthesized ceramics and no other phase is found. The XRD patterns of the $(Sm_{1-x}Lu_x)_3TaO_7$ are very similar to that of Gd_3TaO_7

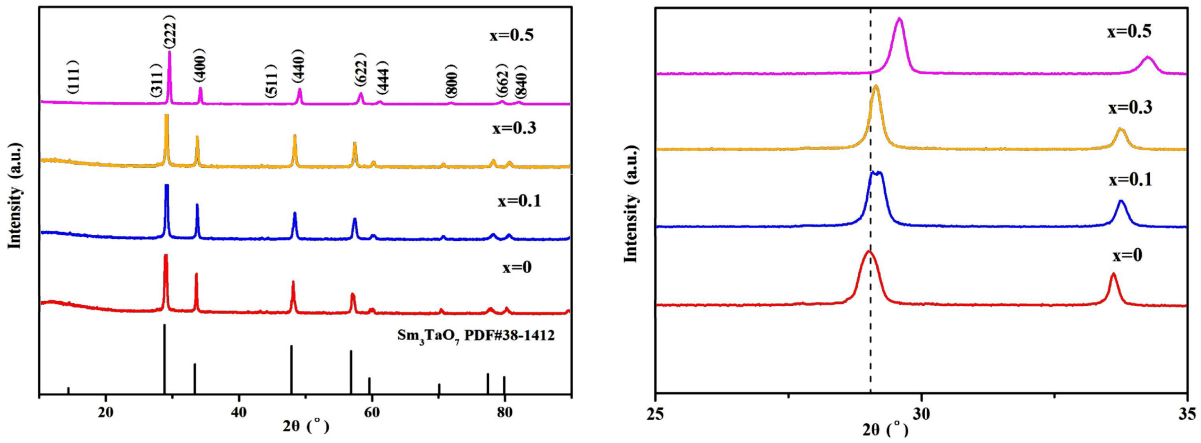

Figure 1. XRD charts of $(Sm_{1-x}Lu_x)_3TaO_7$ ceramics: a) $10° \le 2\theta \le 90°$ and b) $25° \le 2\theta \le 33°$

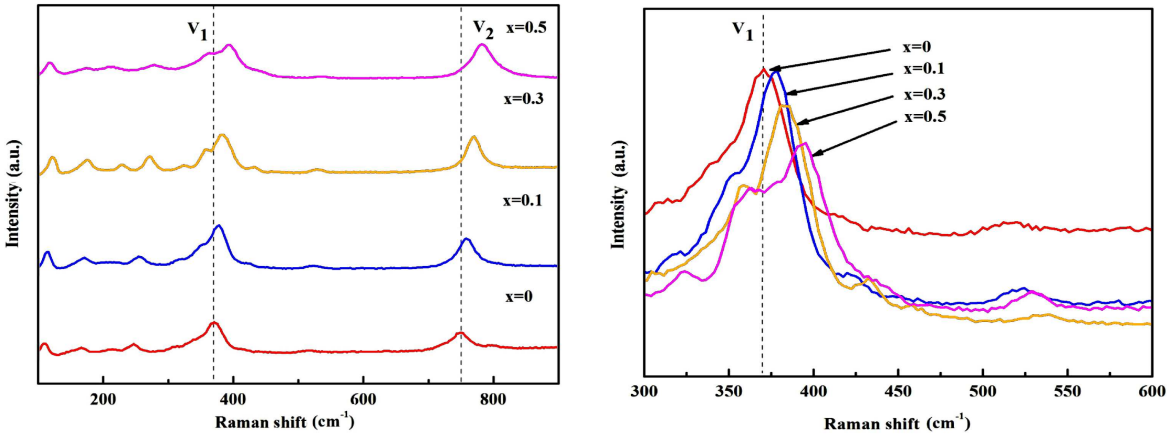

Figure 2. Raman spectrums under 532 nm of $(Sm_{1-x}Lu_x)_3TaO_7$ ceramics: a) normalized Raman spectrums and b) the main Raman peaks

and $La_2Zr_2O_7$ reported in the literature [9,19]. Especially, three typical pyrochlore super-lattice diffraction peaks at 2θ around 14° (111), 28° (311) and 44° (511) indicate that $(Sm_{1-x}Lu_x)_3TaO_7$ ceramics with pure pyrochlore structure are synthesized. XRD patterns of the Lu^{3+} doped samples keep consistence with that of the parent Sm_3TaO_7, which indicates that Lu^{3+} doping does not distort the basic pyrochlore network. Figure 1b shows that the diffraction peaks shift toward higher angle with raising Lu^{3+} content. This phenomenon can be attributed to the decreased average ionic radius of $r(RE^{3+})$, which is computed according to the ionic radius of the chemical constituents by the following equation [20]:

$$r(RE^{3+}) = (1 - x) \cdot r_{Sm^{3+}} + x \cdot r_{Lu^{3+}} \tag{5}$$

The contraction of the unit cell owing to smaller ionic radius of Lu^{3+} (0.098 nm) than that of Sm^{3+} (0.108 nm) means that Lu^{3+} cations have successfully entered the pyrochlore Sm_3TaO_7 lattice according to the Bragg diffraction law [21–23]. From Fig. 1b, the presence of slight peak splitting at 2θ around 29° for the $Sm_{2.7}Lu_{0.3}TaO_7$ can also be observed, which may be ascribed to lattice distortion caused by smaller ion radius Lu^{3+} dopped in Sm_3TaO_7, but the finite doping ratio makes the deviation of the diffraction peak position incompletely.

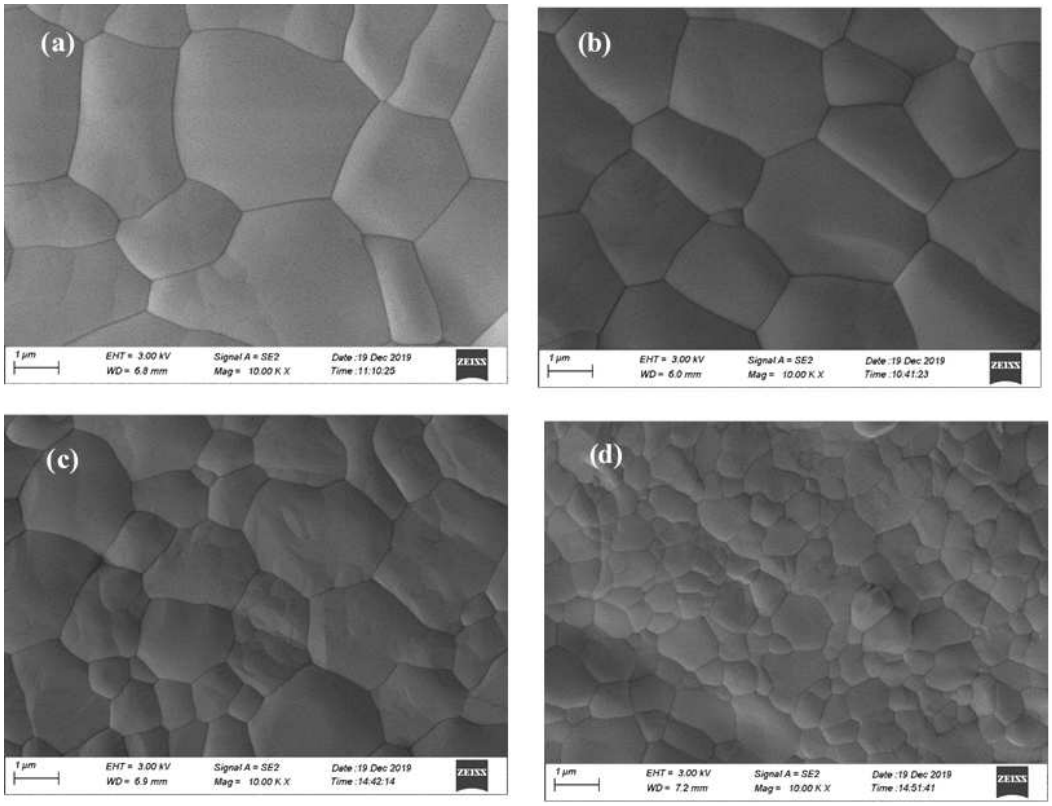

Figure 3. Typical microstructure of $(Sm_{1-x}Lu_x)_3TaO_7$ for x: a) 0, b 0.1, c) 0.3 and d) 0.5

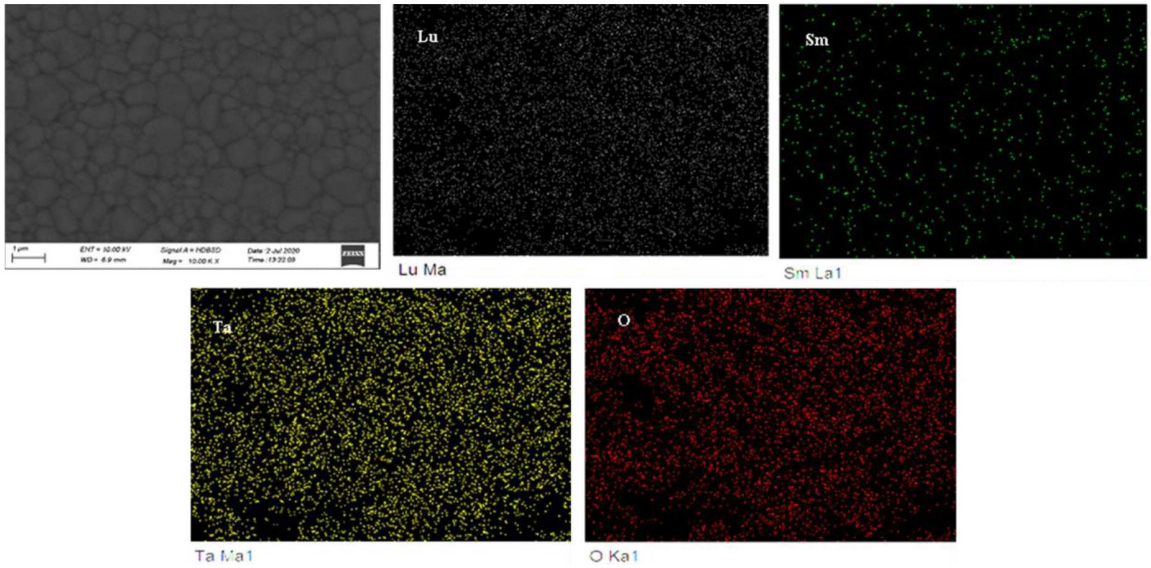

Figure 4. BSE photograph and corresponding surface EDS scanning of $(Sm_{0.5}Lu_{0.5})_3TaO_7$ ceramics

Fig. 2a shows the Raman spectra of the $(Sm_{1-x}Lu_x)_3TaO_7$ ceramics are nearly similar. There are at least six independent Raman characteristic vibration modes around 109, 169, 212, 248, 370 and 749 cm^{-1}, which are similar to that of pyrochlore-type Gd_3TaO_7 [24]. The Raman vibration modes near 100–300 cm^{-1} arise from Sm–O bonds. The Raman peak V_2 belongs to the collinear Ta–O–Ta bonds in TaO_6 octahedra. Obviously, Raman spectra broadening and shifting to higher wavenumber can be observed with increasing Lu contents, and no extra peaks of secondary phase can be found. From Fig. 2b, the intensity of the Raman peak is depressed as Lu^{3+} progressively substitutes for Sm^{3+} ions, which can be attributed to the decreased average ionic radius of $r(RE^{3+})$ and the lattice ordering of $(Sm_{1-x}Lu_x)_3TaO_7$ caused by Lu^{3+} doping [25,26]. From the Raman analysis results, it can also be concluded that Sm^{3+} sites in Sm_3TaO_7 lattice are occupied by Lu^{3+} ions and the $(Sm_{1-x}Lu_x)_3TaO_7$ ceramics exhibit single pyrochlore phase, which is consistent with XRD results.

Typical microstructures of the $(Sm_{1-x}Lu_x)_3TaO_7$ ceramics are shown in Fig. 3. Clearly, the grain boundaries of the $(Sm_{1-x}Lu_x)_3TaO_7$ ceramics are clean and microstructures are quite dense. With the increasing Lu^{3+} content, the grain size decreases gradually from around 5 μm to below 1 μm. The backscattered electron (BSE) photograph and corresponding surface EDS scanning of the $(Sm_{0.5}Lu_{0.5})_3TaO_7$ ceramics are shown in Fig. 4. No second phase is detected, which is in agreement with the results of XRD and Raman. Furthermore, no obvious element agglomeration can be detected and their distribution is homogeneous in samples. Atomic mass percentages of Sm, Lu, Ta and O are 13.32%, 13.08%, 8.92% and 64.68%, respectively. It is basically consistent with stoichiometry of the bulk sample.

3.2. *Optical performance*

UV-Vis diffuse reflectance of $(Sm_{1-x}Lu_x)_3TaO_7$ ceramics (Fig. 5a) increases from 5% to 85% with increasing wavelength. This finding is similar with that of Sm_2O_3 and Sm^{3+} complexes involving in 4*f* energy

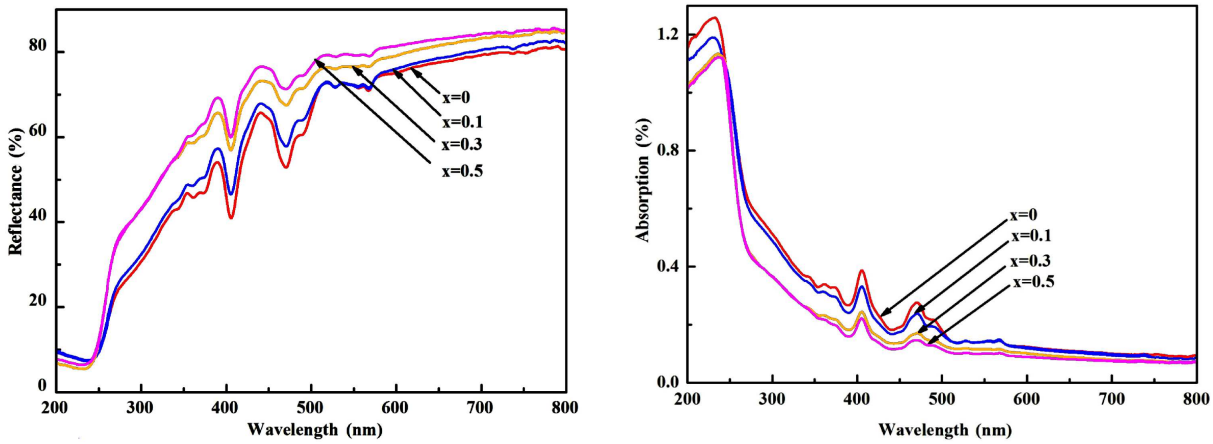

Figure 5. Optical performances of $(Sm_{1-x}Lu_x)_3TaO_7$ ceramics: a) reflectance and b) absorption

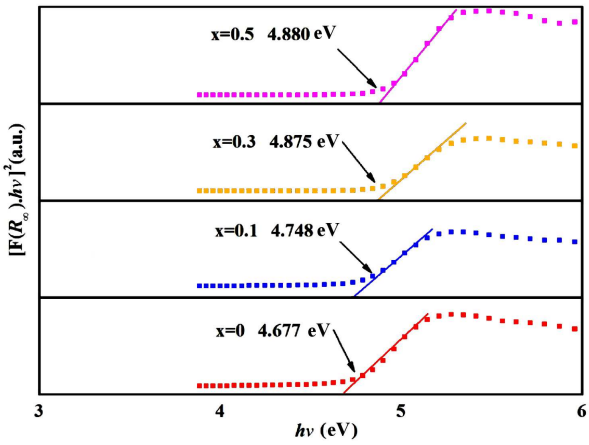

Figure 6. $[F(R_\infty) \cdot h\nu]^2$ vs. $h\nu$ plots of $(Sm_{1-x}Lu_x)_3TaO_7$ ceramics and corresponding band gap values

levels transition and characteristic *f-f* transition of Sm^{3+} cation [12,27]. The absorption variation curves of the samples from 200 to 800 nm are shown in Fig. 5b. Owing to the charge transition from O^{2-} ligands to metallic cations, the absorption is excellent in the UV region just above 250 nm. Due to the thermal radiation resistance being enhanced by excellent absorption of the UV light, graphite films are coated on the $(Sm_{1-x}Lu_x)_3TaO_7$ specimens to weaken thermal radiation before thermal diffusivity measurement.

The band gap (E_g) is derived from extrapolating the linear part of the $[F(R_\infty) \cdot h\nu]^2$ vs. $h\nu$ plot to zero (Fig. 6). With the increasing Lu contents, the value of E_g increases from 4.677 to 4.880 eV. Outstanding insulation performance on the account of the broad band gap shows that the thermal conduction of the $(Sm_{1-x}Lu_x)_3TaO_7$ ceramics is mainly carried by phonons, and influence of the hole and electron conduction should be ignored.

3.3. Thermal conductivity

Calculated specific heat capacities for the $(Sm_{1-x}Lu_x)_3TaO_7$ ceramics increase with temperature rising from 25 to 1400 °C (Fig. 7a). Due to the lower specific heat values of Lu_2O_3 than that of Sm_2O_3 at identical temperature levels, the specific heat capacities decrease with increasing Lu contents. According to Fig. 7b, thermal diffusivities of the samples decrease gradually from 0.777 to 0.254 mm^2/s between 25 and 800 °C, which shows typical feature of phonon heat conduction. The calculated thermal conductivities for the $(Sm_{1-x}Lu_x)_3TaO_7$ ceramics are between 0.95 and 1.44 $W \cdot K^{-1} \cdot m^{-1}$ at 800 °C (Fig. 7c). The thermal diffusivities and conductivities of the $(Sm_{1-x}Lu_x)_3TaO_7$ ceramics are much lower than those of 7YSZ [2] and $Sm_2Zr_2O_7$ [12] and the sample $(Sm_{0.5}Lu_{0.5})_3TaO_7$ has the lowest value.

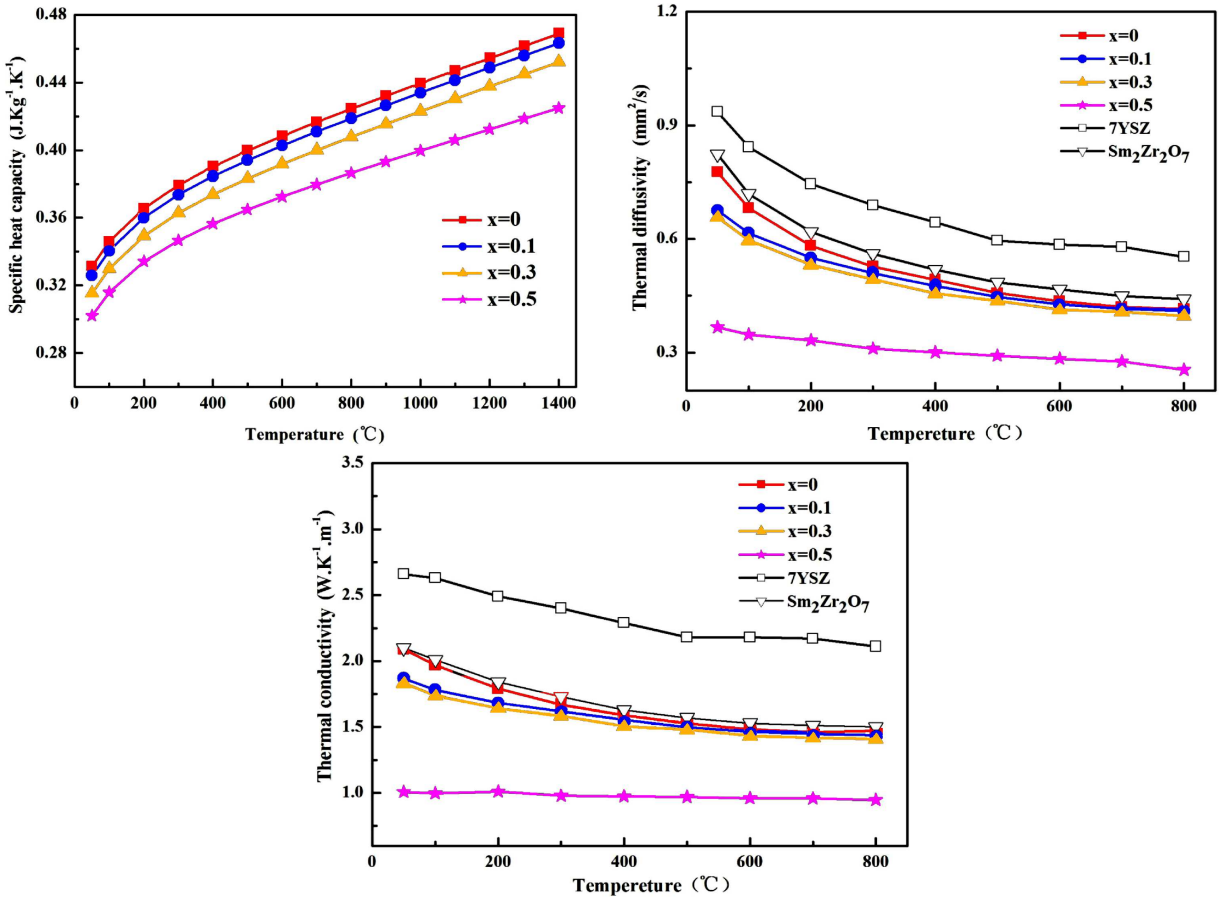

Figure 7. Thermophysical performance of $(Sm_{1-x}Lu_x)_3TaO_7$ ceramics: a) specific heat capacity, b) thermal diffusivity and c) thermal conductivity

Generally, the lattice thermal conductivity is proportional to the mean free path of phonons, which can be influenced by the atomic weight and ion radius differences between the substituted and the substituting ions as expressed by Eqs. 6 and 7 [28,29]:

$$\frac{1}{\tau_{\Delta M}(\omega)} = \frac{c \cdot \alpha^3 \cdot \omega^4}{4\pi \cdot v^3} \left(\frac{\Delta M}{M}\right)^2 \quad (6)$$

$$\frac{1}{\tau_{\Delta R}(\omega)} = \frac{2c \cdot \alpha^3 \cdot \omega^4}{\pi \cdot v^3} \cdot J^2 \cdot \gamma^2 \left(\frac{\Delta R}{R}\right)^2 \quad (7)$$

Here, c, α^3, ω, v, J, γ, M and R are the concentration per atom, atomic volume, the phonon frequency, velocity of transverse wave, the constant and the Gruneisen parameter, the mean atomic weight and inter-ionic distance of the substituting atoms, respectively. ΔM and ΔR are the differences of weight and inter-ionic distance between the substituted and substituting cations, respectively. According to Eqs. 6 and 7, the average free path of phonons can be abated by the elevated ΔM and ΔR, which results in increasing the anharmonic vibration of phonons and enhancing the scattering of phonon.

In light of the XRD and Raman results, structure of the $(Sm_{1-x}Lu_x)_3TaO_7$ can be deemed as the solid solution of Sm^{3+} occupying the Lu^{3+} location in Lu_3TaO_7, or one in which Sm^{3+} is substituted by Lu^{3+} in Sm_3TaO_7. Therefore, the atomic mass and ionic-radius differences between Lu^{3+} and Sm^{3+} can depress the average free path of phonons in the $(Sm_{1-x}Lu_x)_3TaO_7$ ceramics. The smallest average free path can be obtained in when Sm^{3+} and Lu^{3+} are in equal molar ratio in the $(Sm_{1-x}Lu_x)_3TaO_7$ ceramics.

3.4. Thermal expansion performance

Thermal expansion rates of $(Sm_{1-x}Lu_x)_3TaO_7$ ($x > 0$) ceramics increase linearly from room temperature to 1200 °C (Fig. 8a), which arises from the crystal cell expansion and average atom-distance augment with increasing temperature [30]. The phase transition in Sm_3TaO_7 caused by the lattice transformation of Sm_2O_3 is restrained by substituting Lu^{3+} for Sm^{3+} [31], which indicates that the phase transition may be suppressed effectively by cation substitution with the same chemical valence. The linear feature of thermal expansion rates for the $(Sm_{1-x}Lu_x)_3TaO_7$ ($x > 0$) ceramics indicates the excellent lattice stability up to 1200 °C.

As it is shown in Fig. 8b, thermal expansion coefficients (TECs) of the $(Sm_{1-x}Lu_x)_3TaO_7$ ceramics are elevated with increasing Lu contents. Above 800 °C, thermal expansion coefficient of Sm_3TaO_7 decreases abruptly. This may be related to the phase transition from monoclinic to cubic phase of Sm_2O_3 around 850 °C [31]. The $(Sm_{0.5}Lu_{0.5})_3TaO_7$ ($x = 0.5$) sample has the highest TEC of $10.45 \times 10^{-6}\,K^{-1}$ at 1200 °C. Clearly, it is much higher than those of YSZ and $Sm_2Zr_2O_7$ [2,29].

It is well-known that TECs are related to the ionic bond strength [32,33]. According to Eq. 8, the electronegativity difference of A and B ions has direct influence on the ionic bond strength (I_{A-B}) between ions at A and B sites:

$$I_{A-B} = 1 - \exp\left[-\frac{(\chi_A - \chi_B)^2}{4}\right] \quad (8)$$

where χ_A and χ_B are the mean electronegativity at A and B sites. For the $(Sm_{1-x}Lu_x)_3TaO_7$ ceramics, the ions at A sites are Sm^{3+}, Lu^{3+} and Ta^{5+}, the ion at B site is only O^{2-}. The electronegativities of O^{2-}, Sm^{3+}, Lu^{3+} and Ta^{5+} are 3.44, 1.17, 1.27 and 1.5, respectively. Obviously, addition of Lu decreases the value of $\chi_A - \chi_B$, which results in the reduction of I_{A-B}.

Furthermore, the thermal expansion coefficient is reversely proportional to the lattice energy, as it is expressed by the following equation [33]:

$$U = \frac{N_0 \cdot A \cdot z^+ \cdot z^- \cdot e^2}{r_0}\left(1 - \frac{1}{n}\right) \quad (9)$$

where n, r_0, N_0, e, z and A are the Born exponent, inter-ionic distance, the Avogadro's number, charge of

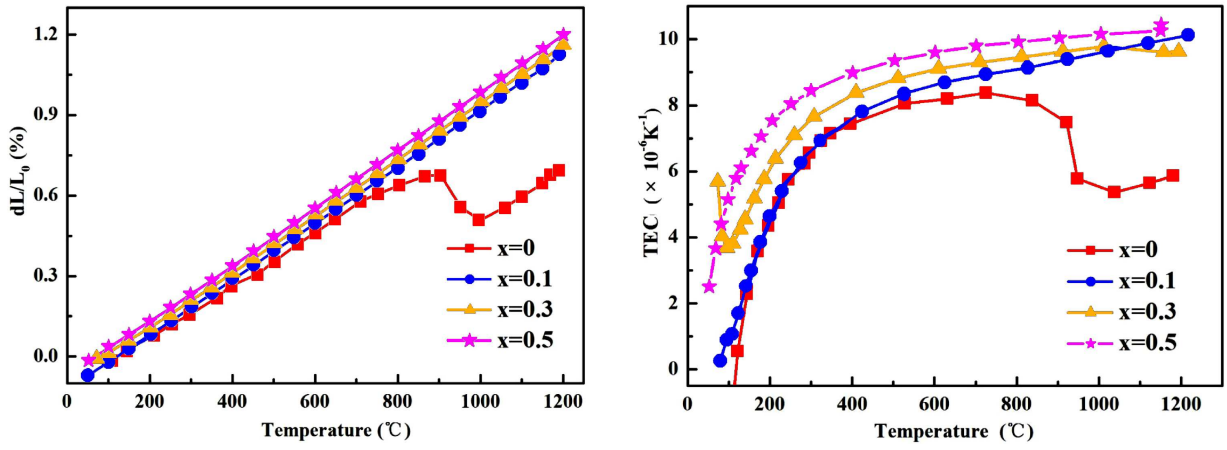

Figure 8. Thermal expansion performance of $(Sm_{1-x}Lu_x)_3TaO_7$ ceramics: a) thermal expansion rate and b) thermal expansion coefficient

an electron, ionic charge and Madelung constant, respectively. Clearly, the lattice energy (U) is reduced by enhanced inter-ionic distance (r_0). Due to the smaller ion radius of Lu^{3+} (0.098 nm) than that of Sm^{3+} (0.108 nm), the inter-ionic distance is increased, which leads to the elevated thermal expansion coefficient in $(Sm_{1-x}Lu_x)_3TaO_7$. Moreover, the crystal lattice energy of oxides decreases with the decreased lattice order degree and increased structural complexity, which also contributes to the elevated thermal expansion coefficient for the obtained samples [34,35]. Therefore, TECs of the $(Sm_{1-x}Lu_x)_3TaO_7$ ceramics are enhanced effectively with increasing Lu contents, which help to reduce the TEC mismatching between TBC materials and superalloy substrate.

IV. Conclusions

$(Sm_{1-x}Lu_x)_3TaO_7$ ceramics (where x = 0, 0.1, 0.3 and 0.5) with single pyrochlore structure are prepared via solid state synthesis and pressureless sintering. Each element distributes uniformly and grain size decreases with the increased value of x. The phase stability is improved effectively by Lu substitution for Sm^{3+}.

Due to the phonon scattering being enhanced by increased differences of the inter-ionic distance and the atomic mass, thermal conductivities of the $(Sm_{1-x}Lu_x)_3TaO_7$ ceramics decrease with increasing Lu contents. The sample $(Sm_{0.5}Lu_{0.5})_3TaO_7$ shows the lowest value (0.95 $W \cdot K^{-1} \cdot m^{-1}$, 800 °C), which is much lower than that for 7YSZ. Because the lattice energy and the average electronegativity difference are reduced as Lu^{3+} substitutes for Sm^{3+}, the TEC of the $(Sm_{0.5}Lu_{0.5})_3TaO_7$ sample achieves the highest value (10.45×10^{-6} K^{-1} at 1200 °C). The thermophysical properties of the prepared $(Sm_{1-x}Lu_x)_3TaO_7$ ceramics satisfy the requirements for thermal barrier coatings.

Acknowledgements: The present works are supported from fund of the National Science Foundation of China (No. U2004182), the Key Project of Science and Technology Research at Henan Province Department of Education (No. 20A5600008), and National Undergraduate Innovation and Entrepreneurship Training Program in Henan Province (No. 202011517015).

References

1. L. Guo, H. Xin, Z. Zhang, X.M. Zhang, F.X. Ye, "Microstructure modification of Y_2O_3 stabilized ZrO_2 thermal barrier coatings by laser glazing and the effects on the hot corrosion resistance", *J. Adv. Ceram.*, **9** [2] (2020) 232–242.
2. W.W. Sang, S.S. Yang, Y. Kang, H.S. Zhang, "Numerical simulation of thermal shock stress of $Sm_2Ce_2O_7$ thermal barrier coatings with different matrix materials", *China Ceram.*, **56** [2] (2020) 45–51.
3. H.S. Zhang, Y.P. Tong, X.F. Yang, W.W. Sang, H.M. Zhang, Y.T. Zhao, "Synthesis and thermophysical performances of complex $Ca_3Ln_3Ti_7Ta_2O_{26.5}$ (Ln = Dy and Er) oxide", *Ceram. Int.*, **46** [3] (2020) 2862–2867.
4. F. Li, L. Zhou, J.X. Liu, Y.C. Liang, G.J. Zhang, "High-entropy pyrochlores with low thermal conductivity for thermal barrier coating materials", *J. Adv. Ceram.*, **8** [4] (2019) 576–582.
5. A. Tang, G.F. Li, Z. Chen, H.S. Zhang, F. Wang, Y.D. Zhao, H.M. Zhang, K. Lu, "Structure characterization and thermophysical properties of R_2LaTaO_7 (R = Dy and Y) oxides", *Ceram. Int.*, **44** [16] (2018) 19160–19164.
6. X.G. Chen, H.D. Li, H.S. Zhang, H.M. Zhang, A. Tang, S. Su, "Influence of Yb substitution for La on thermophysical property of La_2AlTaO_7 ceramics", *Ceram. Int.*, **43** [10] (2017) 7537–7542.
7. J. Yang, Y. Han, M. Shahid, W. Pan, M. Zhao, W.J. Wu, C.L. Wan, "A promising material for thermal barrier coating: pyrochlore-related compound Sm_2FeTaO_7", *Scripta Mater.*, **149** (2018) 49–52.
8. L. Chen, P. Song, J. Feng, "Influence of ZrO_2 alloying effect on thermophyscial properties of fluorite-type Eu_3TaO_7 ceramics", *Scripta Mater.*, **152** (2018) 117–121.
9. Z.L. Xue, Y. Ma, H.B. Guo, "Synthesis, thermal conductivities and phase stability of Gd_3TaO_7 and La doped Gd_3TaO_7 ceramics", *J. Alloys Compd.*, **732** (2018) 759–764.
10. F. S. Wu, P. Wu, L. Chen, F. Jing, "Structure and thermal properties of Al_2O_3-doped Gd_3TaO_7 as potential thermal barrier coating", *J. Eur. Ceram. Soc.*, **39** [6] (2019) 221–2214.
11. H.M. Zhang, Y. Feng, X.G. Chen, H.S. Zhang, Y.X. Liu, A. Tang, B. Ren, "Thermal properties of La_3TaO_7 and La_2AlTaO_7 oxides", *Ceram. Int.*, **43** [1] (2017) 755–759.
12. L. Chen, P. Wu, J. Feng, "Optimization thermophysical properties of TiO_2 alloying Sm_3TaO_7 ceramics as promising thermal barrier coatings", *Int. J. Appl. Ceram. Technol.*, **16** (2019) 230–242.
13. W.K. Sun, Z.P. Zhang, H.F. Liu, W. Wang, X.H. Zeng, "Tailored phase transition temperature and negative thermal expansion of Sc-substituted $Fe_2Mo_3O_{12}$ synthesized by the co-precipitation method", *J. Alloys Compd.*, **794** (2019) 1–7.
14. H. Ikuta, K. Takanaka, M. Wakihara, "The effect of chromium substitution on the phase transition of lithium manganese spinel oxides", *Thermochim. Acta*, **414** [2] (2004) 227–232.
15. A.B. Murphy, "Band-gap determination from diffuse reflectance measurements of semiconductor films, and application to photoelectrochemical water-splitting", *Sol. Energy Mater. Sol. Cells*, **91** [14] (2007) 1326–1337.
16. H.S. Zhang, Y.H. Peng, C.X. Ge, Z.Y. De, J.H. Bin, L. Gang, L.Z. Jun, "Preparation and thermophysical properties of Sm_2YbTaO_7 and Sm_2YTaO_7", *Ceram. Int.*, **42** [13] (2016) 14695–14699.
17. L. Chen, J. Feng, "Influence of HfO_2 alloying effect on microstructure and thermal conductivity of $HoTaO_4$ ceramics", *J. Adv. Ceram.*, **8** [4] (2019) 537–544.
18. Z.F. Zhao, H. Chen, H.M. Xiang, F.Z. Dai, X.H. Wang, W. Xu, K. Sun, Z.J. Peng, Y.C. Zhou, "High entropy defective fluorite structured rare-earth niobates and tantalates for thermal barrier applications", *J. Adv. Ceram.*, **9** [3] (2020) 303–311.
19. H.F. Chen, Y.H. Gao, Y. Liu, H.J. Luo, "Coprecipitation synthesis and thermal conductivity of $La_2Zr_2O_7$", *J. Alloys Compd.*, **480** [2] (2009) 843–848.

20. H. Yamamura, H. Nishino, K. Kakinuma, K. Nomura, "Electrical conductivity anomaly around fluorite-pyrochlore phase boundary", *Solid State Ionics*, **158** [3-4] (2003) 359–365.
21. L. Chen, P. Wu, P. Song, J. Feng, "Synthesis, crystal structure and thermophysical properties of $(La_{1-x}Eu_x)_3TaO_7$ ceramics", *Ceram. Int.*, **44** (2018) 16273–16281.
22. R.D. Shannon, "Revised effective ionic radii and systematic studies of interatomic distances in halides and chalcogenides", *Acta Cryst.*, **A32** (1976) 751–767.
23. L. Chen, P. Wu, P. Song, J. Feng, "Potential thermal barrier coating materials: RE_3NbO_7 (RE = La, Nd, Sm, Eu, Gd, Dy) ceramics", *J. Am. Ceram. Soc.*, **101** [10] (2018) 4501–4508.
24. R. Abe, M. Higashi, K. Sayama, Y. Abe, H. Sugihara, "Photocatalytic activity of R_3MO_7 and $R_2Ti_2O_7$ (R: Y, Gd, La; M: Nb, Ta) for water splitting into H_2 and O_2", *Phys. Chem. B*, **110** [5] (2006) 2219–2226.
25. K.P.F. Siqueira, J.C. Soares, E. Granado, "Synchrotron X-ray diffraction and Raman spectroscopy of Ln_3NbO_7 (Ln = La, Pr, Nd, Sm-Lu) ceramics obtained by molten-salt synthesis", *J. Solid State Chem.*, **209** (2014) 63–68.
26. A. Chesnaud, M.D. Braida, S. Estrade, "High-temperature anion and proton conduction in RE_3NbO_7 (RE = La, Gd, Y, Yb, Lu) compounds", *J. Eur. Ceram. Soc.*, **35** [11] (2015) 3051–3061.
27. G.R. Remya, S. Solomon, J.K. Thomas, A. John, "Sm/YTi(Ta/Nb)O_6: Optical and microwave ceramic composites", *Mater. Today Proc.*, **2** [3] (2015) 1036–1040.
28. Z.G. Liu, J.H. Ouyang, Y. Zhou, "Effect of gadolinia on phase structure and thermal conductivity of ZrO_2-4.5 mol% Y_2O_3 ceramics", *Mater. Lett.*, **62** [20] (2008) 3524–3526.
29. H. Lehmann, D. Pitzer, G. Pracht, R. Vassen, D. Stöver, "Thermal conductivity and thermal expansion coefficients of lanthanum rare-earth-element zirconates system", *J. Am. Soc. Ceram.*, **86** [8] (2003) 1338–1344.
30. Z.G. Liu, J.H. Ouyang, Y. Zhou, "Structural evolution and thermophysical properties of $(Sm_xGd_{1-x})_2Zr_2O_7$ ($0 \leq x \leq 1.0$) ceramics", *J. Alloys Compd.*, **472** [1-2] (2009) 319–324.
31. S. Mochizuki, "Intense white luminescence of Sm_2O_3 irradiated with ultraviolet laser light under vacuum", *Physica B*, **340-342** (2003) 944–948.
32. H.S. Zhang, Z.J. Li, Q. Xu, F.C. Wang, L. Liu, "Preparation and thermophysical properties $Sm_2(Ce_{0.3}Zr_{0.7})_2O_7$ ceramic", *Adv. Eng. Mater.*, **10** [1-2] (2008) 139–142.
33. Z.X. Qu, C.L. Wan, W. Pan, "Thermophysical properties of rare-earth stannates: Effect of pyrochlore structure", *Acta Mater.*, **60** [6-7] (2012) 2939–2949.
34. L.M.T. Martínez, M.A.R. Gómez, E. Moctezuma, "Features of crystalline and electronic structures of Sm_2MTaO_7 (M = Y, In, Fe) and their hydrogen production via photocatalysis", *Ceram. Int.*, **43** [5] (2017) 3981–3992.
35. Z. Ma, Q. Zhang, L. Liu, Y.B. Liu, "Preparation and heat insulating capacity of $Sm_2Zr_2O_7$-SiC composites based on photon thermal transport", *J. Adv. Ceram.*, **9** [4] (2020) 454–461.